The obligate intracellular bacterium *Orientia tsutsugamushi* differentiates into a developmentally distinct extracellular state

Sharanjeet Atwal[b*], Jantana Wongsantichon[a*], Suparat Giengkam[a*], Kittirat Saharat[a], Yanin Jaiyen[a], Suthida Chuenklin[b], Taerin Chung[c], Hyun Huh[c], Sang-Hyuk Lee[c,d], Radoslaw M. Sobota[e] and Jeanne Salje[a, b, f#]

Mahidol-Oxford Tropical Medicine Research Unit, Faculty of Tropical Medicine, Mahidol University, Bangkok, Thailand[a]

Public Health Research Institute, Rutgers the State University of New Jersey, Newark, USA[b]

Institute for Quantitative Biomedicine, Rutgers University, Piscataway, New Jersey 08854, USA[c]

Department of Physics and Astronomy, Rutgers University, Piscataway, New Jersey 08854, USA[d]

Institute of Medical Biology, Agency for Science, Technology and Research (A*STAR), 138648, Singapore[e]

Centre for Tropical Medicine and Global Health, Nuffield Department of Medicine, University of Oxford, Oxford, United Kingdom[f]

* These authors contributed equally

[#] Address correspondence to Jeanne Salje: js2522@rutgers.edu

Abstract

Orientia tsutsugamushi (Ot) is an obligate intracellular bacterium in the family Rickettsiaceae that causes scrub typhus, a severe mite-borne human disease. Ot is unusual amongst Rickettsiaceae in budding out of infected cells in a process resembling that used by enveloped viruses. Here, we show that Ot bacteria that have budded out of host cells are in a distinct developmental stage compared with intracellular bacteria. We refer to these two stages as intracellular and extracellular bacteria (IB and EB, respectively). These two forms differ in physical properties: IB is elongated, and EB is round. Additionally, IB has higher levels of peptidoglycan and is physically robust compared with EB. The two bacterial forms differentially express proteins involved in bacterial physiology and host-pathogen interactions, specifically those involved in bacterial dormancy and stress response, secreted bacterial effectors, and outer membrane autotransporter proteins ScaA and ScaC. Whilst both populations are infectious, entry of IB Ot is sensitive to inhibitors of both clathrin-mediated endocytosis and micropinocytosis, whereas entry of EB Ot is only sensitive to a micropinocytosis inhibitor. Our identification and detailed characterization of two developmental forms of Ot significantly advances our understanding of the intracellular lifecycle of an important human pathogen.

Keywords

Orientia tsutsugamushi, Rickettsiales, obligate intracellular bacteria, intracellular pathogens

Author Summary

Orientia tsutsugamushi (Ot) is a bacterial pathogen that causes scrub typhus, a mite-transmitted human disease. This illness is traditionally known to be endemic in the Asia-Pacific, but recent reports from the Middle East, Africa, and Latin America suggest that it may be globally distributed. Scrub typhus is associated with high mortality if not treated promptly with appropriate antibiotics. Ot is a highly specialized bacterium that can only replicate within living cells, either within the mite vector or in mammalian or human hosts. Ot exits infected cells using a unique mechanism that involves budding off the surface of infected cells. We have discovered that this unusual aspect of its lifecycle involves the bacteria themselves differentiating into a distinct growth form. Different growth forms have not been described in other members of the family Rickettsiaceae, and no other family members have been shown to bud out of host cells in a manner similar to Ot. We find that the two forms of Ot, which we refer to as intracellular and extracellular bacteria (IB and EB respectively), differ in physical properties and protein expression and infect cells through different mechanisms. The identification of structurally and functionally distinct forms of Ot elucidates a vital aspect of this pathogen's intracellular life cycle. Our findings are likely to advance the development of novel interventions aimed at inhibiting Ot growth in scrub typhus patients.

62 **Main**

63 *Orientia tsutsugamushi* (Ot) is an obligate intracellular Gram-negative bacterium that causes the
64 mite-transmitted human disease scrub typhus. This condition is one of the most severe rickettsial
65 diseases; it is associated with a median 6% mortality in untreated patients[1]. Scrub typhus is a
66 leading cause of severe febrile illness in the Asia-Pacific, a region containing two-thirds of the
67 world's population. Recent reports from Latin America, the Middle East, and Africa suggest that
68 the disease is more globally distributed[2]. Knowledge of the fundamental biology of this organism
69 lags behind that of pathogens of equivalent prevalence and severity. Historical underestimations
70 of Ot incidence, its classification as a biosafety level 3 pathogen, its fastidious growth in cultured
71 cells, and the fact that it remains genetically intractable[3] likely account for the paucity of studies
72 focused on this pathogen.

73 The order Rickettsiales contains two major families: Anaplasmataceae and Rickettsiaceae[4].
74 Members of the Anaplasmataceae, which include *Anaplasma* spp. and *Ehrlichia* spp., reside
75 within membrane-bound vacuoles inside host cells. The developmental cycle of certain
76 Anaplasmataceae family members is biphasic and involves switching between a non-infectious
77 intracellular replicative form (reticulate body) and an infectious extracellular form (elementary
78 body). While members of the Rickettsiaceae, namely *Rickettsia* spp. and Ot, do not appear to
79 differentiate into distinct forms during their intracellular lifecycle, Ot buds out of host cells in a
80 manner reminiscent of enveloped viruses[5]. This observation led us to investigate whether budded
81 Ot is in a distinct developmental stage compared with intracellular counterparts.

82 Ot has been shown to enter host cells using the zipper-like invasion mechanism, which is common
83 to many Rickettsiales members[4]. This process is initiated by binding of bacterial surface adhesins
84 to receptors expressed on mammalian cells. Adhesins such as TSA56, ScaA, and ScaC[6-8] bind
85 to host cell fibronectin and syndecan-4; these proteins then interact with integrin α5ß1, leading to
86 activation of intracellular signaling that culminates in actin remodeling and clathrin-mediated

87 endocytosis[9-11]. It is important to emphasize that these studies were entirely focused on
88 intracellular Ot, as they were performed on bacteria isolated from host cells by mechanical lysis
89 of infected cells. However, the re-entry mechanism utilized by bacteria that have budded out of
90 cells may be influenced by the presence of an enveloping host cell membrane and/or its
91 differentiation into a distinct state.

92 Here, we show that Ot exists in distinct intracellular (IB) and extracellular (EB) bacterial
93 populations. We report the characterization of these two states in terms of their physical
94 properties, metabolic activity, and gene expression profiles and demonstrate that they enter host
95 cells using different mechanisms.
96

97 **Results**

98 **IB and EB forms of Ot differ in physical properties and metabolic activity.**

99 Ot is typically described as a coccobacilli bacterium. Its small size and propensity to aggregate
100 make it difficult to obtain clear images of this bacterium using conventional light microscopy. To
101 circumvent this challenge, we labelled Ot with an antibody against the abundant surface protein
102 TSA56 and employed stochastic optical reconstruction microscopy (STORM) for high-resolution
103 imaging. We first investigated the shape of bacteria located inside and outside host cells (Fig. 1A,
104 B and Supp. Fig 1). We found that EBs were approximately round in shape with a diameter of
105 about 1.2 μm. In contrast, IBs adopted diverse round and elongated shapes and varied in
106 dimensions; some bacteria were 3-4 μm in length. Additionally, IB size varied during the course
107 of infection. Initially, and up to one-day post-infection, IBs and EBs were similar in length. At later
108 stages, *i.e.,* 2-7 days following infection, IBs were characterized by longer lengths. These kinetic
109 changes in shape correlated with Ot growth dynamics whereby replication starts 24-48 hours
110 point infection[12]. These differences in shape provide evidence for the existence of two separate
111 bacterial forms.

112 We next investigated potential differences in bacterial cell wall composition. We previously
113 showed that Ot builds a low-abundance peptidoglycan-like structure[13]. Thus, we assessed relative
114 peptidoglycan levels in IB and EB Ot forms using a NOD-1 reporter assay (Fig. 1C). We detected
115 significantly more peptidoglycan in IB cells compared with EB cells. This finding may account for
116 the observed differences in shape (Fig. 1A) as peptidoglycan is required to build elongated cells.

117 In related structural studies, we capitalized on our previous finding that the abundant surface
118 protein TSA56 is involved in forming disulfide bonds with itself or other proteins, leading to the
119 formation of aggregates[13]. These complexes can be identified as smears following sample
120 preparation in the absence of reducing agents and evaluation by immunoblot analyses. In this
121 study, we found evidence for substantially higher disulfide bond formation in EB Ot than IB Ot, as

122 determined by the presence of a high molecular weight smear (Fig. 1D). We hypothesize that this
123 crosslinked structure confers EB Ot with additional structural rigidity in the absence of
124 peptidoglycan. These experiments were performed in the presence of iodoacetamide, an agent
125 that covalently modifies cysteine residues and prevents them from forming new bonds, thus
126 ensuring that the cross-links were not formed during sample preparation and processing.

127 Our next goal was to assess potential changes in genome copy number as, during rapid growth,
128 bacteria such as *E. coli* carry multiple genome copies within a single cell. To address this issue,
129 we determined bacterial cell numbers using fluorescence microscopy and bacterial genome
130 copies using qPCR. We found no differences: Ot IB and EB harbored just over one estimated
131 genome copy per cell (Fig. 1E). This measurement is an approximation that suffers limitations
132 associated with absolute quantification using qPCR and microscopy, but any such errors are
133 expected to be constant between the IB and EB measurements.

134 Finally, we asked whether IB and EB Ot forms differed in their metabolic activity. Ot is an obligate
135 intracellular bacterium with limited central metabolic and biosynthetic capability[14] and a reliance
136 on host cells for carbon and nitrogen sources and metabolic intermediates. These observations
137 led us to hypothesize that EB bacteria are metabolically inactive owing to their extracellular
138 location. To test this, we used a microscopy-based assay whereby growing bacteria are exposed
139 to a clickable methionine analog L-Homopropargylglycine (HPG). that is subsequently labeled
140 with a fluorophore[15] (Fig. 1F). Using this methodology, we observed that 86% of IB were
141 translationally active five days post-infection, compared with 0% of EB (Fig. 1G). It is possible that
142 EB Ot undergo some residual metabolic activity that is not detected by our assay of protein
143 translation. The fact that not all IB were labelled with HPG indicated that this result did not simply
144 reflect a difference in bacterial permeability between the IB and EB forms. These results provide
145 an additional line of evidence to support the existence of two fundamentally different Ot states.
146

147 **IB and EB forms of Ot exhibit different gene and protein expression profiles.**

148 We next investigated whether the differences in physical properties and metabolic activity
149 observed in IB and EB forms of Ot were accounted exclusively by physical location relative to
150 host cells. Exposure of EB forms to an osmotically different extracellular environment combined
151 with the lack of nutrient availability might account for our observations. However, a second
152 possibility is that EB forms arise by differentiation of IB into a biochemically distinct state. We
153 reasoned that bacteria in the same developmental stage but differing in position relative to host
154 cells would exhibit almost identical protein profiles. To test this, we performed shotgun mass
155 spectrometric analyses on isolated IB and EB Ot forms. We found (Supp. Fig. 2) that IB and EB
156 isolated four days post-infection exhibited distinct protein profiles (correlation coefficient = 0.843).
157 A complete list of proteins differentially expressed is provided in Supp. Table 1. Pathway analyses
158 revealed that IB Ot was enriched in proteins involved in protein synthesis (Fig. 2A). In contrast,
159 EB Ot displayed high expression of SpoT and RpoH, two proteins involved in dormancy and
160 quiescence (Fig. 2B). Additionally, we observed striking differential expression of effector
161 proteins: multiple Ankyrin repeat-containing proteins (Anks) were enriched in IB Ot, whereas
162 tetratricopeptide repeat-containing proteins (TPRs) were enriched in EB Ot (Fig. 2C).

163 We next investigated whether EB and IB Ot exhibited differences in transcript expression levels.
164 These experiments required the propagation of large amounts of EB because this form of Ot is
165 metabolically inactive and thus harbors very low mRNA levels. We selected 12 genes, three of
166 which (*curA, trxB, sodB*) were expressed at similar levels in our proteomic studies comparing EB
167 and IB. Additionally, we quantified mRNA expression of five genes encoding proteins enriched in
168 IB Ot (*yccA, nuoB, dapA, ank12, scaA*) and four genes enriched in EB Ot (*obgE, spot, tsa56*). We
169 isolated RNA from IB and EB bacteria four days post-infection and assessed mRNA levels by
170 qRT-PCR (Fig. 2D). We found no correlation between mRNA and protein levels in multiple cases.
171 For example, RpoH transcript levels were similar in IB and EB Ot, but protein expression was

172 higher in EB. These observations provide additional evidence supporting the existence of
173 molecularly distinct bacterial forms and suggest that transcriptional and post-transcriptional
174 regulatory mechanisms participate in the differentiation process.
175
176 **Surface proteins are differentially expressed on IB and EB forms of Ot.**
177 Our differential proteomics analyses revealed that IB and EB differentially express specific surface
178 proteins (Fig. 3A). Surface proteins play a central role in Ot function for two reasons. First, unlike
179 most Gram-negative bacteria, Ot lacks lipopolysaccharide, which generally serves as a
180 membrane shield. Second, Ot is a cytosolic bacterium, and its surface is in direct contact with
181 cytoplasmic host components. Ot harbors genes encoding four widely conserved autotransporter
182 proteins: ScaA, ScaC, ScaD, and ScaE. Using our proteomics dataset, we detected ScaA and
183 ScaC, but not ScaD or ScaE. ScaA was slightly enriched in IB relative to EB Ot (1.5X), while ScaC
184 was enriched in EB (1.87X). Ot also harbors genes encoding three immunogenic surface proteins
185 that dominate the humoral response in human patients, TSA22, TSA47, and TSA56. We found
186 that TSA22 was enriched in IB relative to EB Ot (3.2X) while TSA47 and TSA56 were not
187 significantly differentially expressed (1.14X and 1.32X increase in EB compared with IB,
188 respectively). To verify our protein expression observations, we generated polyclonal antibodies
189 against ScaA and ScaC and determined their expression in IB and EB bacteria using immunoblot
190 analyses (Fig. 3B). Our experiments up to this point were performed in mouse fibroblasts (L929)
191 because Ot grows readily in these cells. Moreover, L929 fibroblasts are suitable for characterizing
192 bacterial properties that are not affected by the cellular environment. However, for our validation
193 studies, we also investigated bacteria grown in primary human umbilical vein endothelial cells
194 (HUVEC) as a more physiologically relevant model of Ot infection in humans. Our immunoblot
195 studies in both L929 and HUVECs confirmed enrichment of ScaA in IB Ot and higher expression
196 of ScaC in EB compared to IB Ot, in agreement with our mass spectrometric analyses.

197

198 **ScaA and ScaC as markers of EB and IB forms of Ot**

199 Our observation that 86% of IB is translationally active five days post-infection, compared with
200 0% of EB, combined with the fact that these Ot forms display opposite ScaA and ScaC expression
201 led us to investigate whether these surface proteins can be used as *bonafide* markers of
202 metabolically active IB and metabolically quiescent EB Ot forms, respectively. We used
203 immunofluorescence microscopy to identify bacteria expressing ScaA and ScaC and then
204 quantified the number of translationally active ScaA- and ScaC-positive bacteria by measuring
205 incorporation of L-Homopropargylglycine (HPG). We found (Fig. 3C) that ScaA-positive bacteria,
206 in contrast to ScaC-positive Ot, were mostly translationally active. We then quantified the number
207 of ScaA/ScaC positive bacteria inside and outside cells and confirmed that ScaC and ScaA
208 expression were upregulated in EB and IB Ot, respectively (Fig. 3D, E). Together, these results
209 show that ScaA and ScaC are differentially expressed depending on bacterial location relative to
210 host cells: metabolically active IB express higher levels of ScaA relative to EB Ot. Conversely,
211 expression of ScaC in metabolically inactive EB is high relative to that of IB forms of Ot.

212 The observation that EB expressed high ScaA transcript levels (Fig. 2E) but low levels of ScaA
213 protein led us to hypothesize that ScaA is translated into protein soon after entry into host cells,
214 using pre-formed mRNA. We quantified the number of IB Ot expressing ScaA and ScaC at 1 and
215 3 hours post-infection and found a decrease in ScaC expression and an increase in ScaA
216 expression as the infection proceeded (Fig. 3F). These results show that ScaA is expressed
217 during the first 3 hours after infection, suggesting that *scaA* transcripts are made in EBs in
218 anticipation of new infections. These results point to the existence of regulatory mechanisms that
219 control the expression of ScaA and ScaC on the surface of Ot cells, depending on bacterial
220 location and stage of host infection.

221

222 **IB and EB Ot populations are infectious but differ in physical stability and mechanisms of**
223 **entry into host cells.**

224 Previous studies have shown that specific Anaplasmataceae differentiate into distinct intracellular
225 and extracellular forms and that only the extracellular form is effective at infecting host cells[16].
226 This observation led us to investigate whether the ability to infect host cells differs in IB compared
227 with EB Ot. Growth curve measurements revealed that both bacterial forms could infect cells and
228 replicate with similar dynamics (Fig. 4A). However, IB appears to retain infectivity more efficiently
229 than EB following physical and osmotic challenges. Specifically, when we subjected IB and EB
230 Ot to physical stress using a bead mill for 1-2 minutes, we found that EB displayed a reduction in
231 growth that was dependent on the time of exposure to stress; in contrast, IB was unaffected by
232 this treatment (Fig. 4B). Furthermore, osmotic shock resulted in a significantly greater reduction
233 in viability in EB compared with IB (Fig. 4C). Together, these results demonstrate that IB is
234 physically more robust than EB; this property is likely due to differences in peptidoglycan content,
235 as described above.

236 To investigate whether EB and IB forms of Ot enter host cells using the same invasion
237 mechanism, we pre-treated HUVEC cells with the clathrin-mediated endocytosis inhibitor
238 dynasore or the micropinocytosis inhibitor amiloride. We then infected the cells with IB or EB Ot
239 and quantified the number of intracellular bacteria 3 hours post-infection using confocal
240 microscopy (Fig. 4D, E). The entry of IB Ot into the cells was blocked by dynasore, thus confirming
241 the participation of clathrin-mediated endocytosis in this process. IB entry was also partially
242 inhibited by amiloride, suggesting additional involvement of micropinocytosis in bacterial uptake.
243 In contrast, EB Ot entry into cells was not affected by dynasore treatment but was completely
244 inhibited by pre-incubation with amiloride. These results demonstrate that IB and EB forms of Ot
245 use distinct mechanisms of entry into host cells. Our findings were recapitulated in L929

246 fibroblasts (Supp. Fig. 6), thus establishing that EB Ot enters cells through macropinocytosis,
247 whereas IB Ot utilizes both clathrin-mediated endocytosis and macropinocytosis.
248

249 **Discussion**

250 Our studies have unveiled a new feature of the obligate intracellular bacterium Ot. This organism's
251 unique exit strategy, which involves budding off the surface of infected cells, is associated with
252 differentiation into a molecularly and functionally distinct developmental state. While unusual in
253 the family Rickettsiaceae, this property is reminiscent of the biphasic lifecycle of multiple species
254 in the sister family Anaplasmataceae[4] and the unrelated obligate intracellular bacteria *Chlamydia*
255 spp.[17] and *Coxiella burnettii*[18]. However, in contrast to these organisms, Ot resides in the host
256 cytosol in naked form rather than in a membrane-bound vacuole. To our knowledge, this is the
257 first description of an intracellular bacterium living freely in the host's cytosol and having a biphasic
258 lifecycle. Our findings have important implications for our understanding of Ot biology and unveil
259 opportunities to develop better therapeutic strategies to treat scrub typhus.

260 The physical properties of prokaryotic cell walls are crucial for survival. These stiff structures
261 maintain cellular shape, protect the interior, counteract osmotic pressure, and provide structural
262 strength through peptidoglycan layers. Our studies revealed that EB and IB forms of Ot differ in
263 peptidoglycan content. Lower levels in EB compared with IB make this form more susceptible to
264 physical and osmotic stress. There is a long-standing question regarding the role of peptidoglycan
265 in obligate intracellular bacteria. These organisms reside in an osmotically protective niche and
266 are under selective pressure to reduce the abundance of immunogenic pathogen-associated
267 molecular patterns (PAMP)s[19]. In the case of pathogenic *Chlamydia* species, it has been shown
268 that peptidoglycan is retained only at the septum and is required for cell division[20]. Higher

269 peptidoglycan levels in IB Ot *vs.* EB Ot point to the retention of peptidoglycan for growth and
270 division rather than structural integrity maintenance.

271 The observed differences in physical properties between EB and IB forms are complemented with
272 distinct protein expression profiles suggesting that each form performs unique functions or
273 responds to specific challenges. Proteomics analyses in EB Ot revealed increased expression of
274 heat shock sigma factor RpoH and the alarmone (p)ppGpp synthetase SpoT associated with the
275 stringent response[21]. These results suggest that the EB form of Ot shares features with the
276 dormant state of other bacteria. Notably, Ot is the only reported member of the Rickettsiaceae to
277 encode a full-length *spoT* gene[4]. This exclusive feature is in harmony with the fact that
278 developmental differentiation of Ot is highly unusual in members of this family. The changes
279 associated with differentiation into the EB state likely serve one or both of the following purposes:
280 ensuring survival in the extracellular state and priming the bacteria for reinfection of new cells.
281 Indeed, the observation that *scaA* transcripts are abundant in the EB form and that ScaA protein
282 is synthesized early upon entry into host cells supports the idea that EB Ot is primed for infection.

283 Comparing the protein and RNA transcript levels of selected genes revealed a poor correlation
284 for many genes. A potential explanation is that RNA levels are low in the metabolically inert EB
285 form, which does not reflect newly translated proteins. Ot strain UT76 encodes only 8 predicted
286 transcription factors and two sigma factors, RpoD and RpoH[22]. Thus, it is possible that gene
287 expression is not strictly regulated at the transcriptional level but that other forms of regulation are
288 prevalent in Ot. We recently showed high antisense transcription levels in Ot, especially in genes
289 associated with the rampant integrative conjugative element RAGE, which dominates the Ot
290 genome[23]. There, we found that high antisense transcription correlates with low protein levels for
291 a particular gene, pointing to this mechanism as a central regulatory strategy in Ot. Gene
292 expression in the Ot-related, free-living alphaproteobacterium *Caulobacter crescentus* is highly

293 regulated by proteolysis[24]. Mechanisms based on differential proteolysis may therefore also play
294 an essential role as critical determinants of protein expression in Ot.

295 Our observation that EB Ot enters cells through pinocytosis, whereas IB Ot utilizes endocytosis
296 and, to a lesser extent, pinocytosis resolves a long-standing gap in the field as it was unclear how
297 budded bacteria enveloped in plasma membrane enter host cells. Physiologically, IB entry into
298 host cells may be necessary during trafficking into adjacent cells, as previously described for
299 spotted fever group *Rickettsia* spp.[25]. Additionally, low levels of cell may release IB Ot forms that
300 can then infect new host cells. The different mechanisms utilized by EB and IB to enter cells
301 suggest that strategies to escape from the endolysosomal pathway will differ between the two Ot
302 forms. It is unclear whether and how the differing transcriptional and proteomic profiles at the
303 point of infection will affect early host-pathogen interactions. Our finding that IB and EB's growth
304 dynamics are similar suggests that early differences do not persist through the infection cycle.

305 In summary, our finding that Ot differentiates into molecularly and functionally distinct forms
306 provides a novel framework to study the infection cycle of this important obligate intracellular
307 pathogen and opens avenues to investigate the physiological significance of the distinct
308 populations characterized.

309

310 **Fig. 1: Intracellular and extracellular forms of Ot are physically and metabolically distinct**.
311 A. STORM images of IB and EB Ot in L929 cells. Bacteria were labelled with a monoclonal
312 antibody against surface protein TSA56. Additional images are provided in Supp. Fig. 1. B. Length
313 quantification of individual IB and EB Ot as imaged by STORM. C. Quantification of relative
314 peptidoglycan levels through activation of NOD1 reporter cells, as measured by secreted alkaline
315 phosphatase activity. EB Ot induced less activation than IB, indicating lower levels of
316 peptidoglycan. Identical amounts of IB and EB Ot were used, and biological triplicates are shown.
317 D. Immunoblot showing the formation of disulfide cross-linked aggregates of the surface protein
318 TSA56, observed in the absence of the reducing agent beta-mercaptoethanol (BME). This effect
319 was stronger in EB compared with IB Ot. The expected molecular weight of TSA56 (56 kDa) is
320 indicated with an arrow, and a dashed arrow depicts higher-order aggregates. E. Genome copy
321 number per cell as measured by qPCR; bacterial cell number was determined by
322 immunofluorescence microscopy. Quantification of 10 individual imaging fields is shown. F.
323 Confocal microscopy image of an L929 cell infected with Ot and labelled with the clickable
324 methionine analog homopropargylglycine (HPG, green) and an antibody against surface protein
325 TSA56 (red). The host cell outline is showed by a dashed line, and an arrow indicates a
326 metabolically inactive bacterium located outside the host cell. G. Quantification of metabolic
327 activity, as measured by a detectable HPG signal, in IB and EB Ot. L929 cells were infected with
328 Ot for five days, fixed, and labelled with TSA56 and HPG. One-hundred bacteria inside (IB) and
329 outside cells (EB) were counted and scored as being HPG-positive or -negative. The percentage
330 of HPG-positive IB and EB Ot, based on individual values from three independent replicates.
331 Statistical significance (t-test) was determined using Graphpad Prism software. p-value *** ≤
332 0.001.
333
334 **Fig. 2: Intracellular and extracellular forms of Ot have distinct gene expression profiles.**

335 A. Pathway analysis of proteins upregulated >2X between IB and EB forms of Ot (60 proteins in
336 IB, 47 proteins in EB). Bacteria were grown in L929 cells at an MOI of 410:1 and harvested four
337 days post-infection. IB and EB Ot were isolated and analysed by shotgun proteomics. B. SpoT
338 and RpoH are upregulated in EB compared with IB Ot as measured by proteomics described in
339 A. C. Differential expression of Ankyrin-repeat-containing proteins (Anks) and tetratricopeptide
340 repeat-containing proteins (TPR) in EB and IB Ot measured by proteomics, as in A. D. RTqPCR
341 analysis showing relative levels of 12 genes expressed in EB and IB Ot. Bacteria were isolated
342 from L929 cells four days post-infection at an MOI of 672:1, 300:1, and 560:1. The figure depicts
343 results from three independent replicates. Gene expression levels were normalised using three
344 genes: *mipZ*, *ank12*, and *16S.* Mean and standard deviation values are shown. The ratio of protein
345 levels in EB/IB, as found in the proteomics experiment in 2A, is given above each gene for
346 comparison.
347
348 **Fig. 3: Autotransporter proteins ScaA and ScaC are differentially expressed on IB and EB**
349 **forms of Ot.**
350 A. Volcano plot showing differential expression of surface proteins in proteomics analysis of IB
351 and EB forms of Ot. We observed higher expression of ScaC, TSA56, and TSA47 in EB whilst IB
352 Ot expressed higher ScaA and TSA22 levels B. Immunoblot analysis of IB and EB Ot from
353 infected L929 and HUVEC cells confirming differential expression of ScaA, and ScaC between IB
354 and EB forms. Loading was normalised by measuring bacterial genome copy number using qPCR
355 and loading the same number of IB and EB Ot in each pairwise comparison. Uncropped
356 immunoblot images showing antibody specificity are given in Supp. Fig. 3. C. Quantification of
357 translational activity, as determined by a positive confocal microscopy signal observed with the
358 clickable methionine probe L-homopropylgylglycine (HPG). L929 cells were infected with Ot for
359 five days, then fixed and labelled with HPG and anti-ScaA or anti-ScaC antibodies. ScaA/ScaC-
360 positive bacteria were scored as being positive or negative for HPG labelling. Mean and SD of

361 three independent replicates are shown. D. Confocal microscopy images of HUVEC cells infected
362 with Ot for five days and labelled for DNA (hoescht, blue), translational activity (HPG, green),
363 ScaA (anti-ScaA antibody, magenta) and ScaC (anti-ScaC antibody, red). Scale bar = 10 µm.
364 Examples of extracellular bacteria labelled with ScaC are shown with a white arrow. More images
365 as well as equivalent experiments in L929 cells are shown in Supplementary Figures 4 and 5. E.
366 Quantification of confocal micrographs of HUVEC cells infected with Ot and labelled as in 3D.
367 The percentage of IB and EB Ot at five days post-infection that were positively labelled with anti-
368 ScaA and -ScaC antibodies was counted in three independent experiments. Graph shows mean
369 and SD, and p value determine by unpaired t test. F. Quantification of ScaA- and ScaC-positive
370 IB bacteria inside HUVEC cells one and three hours post-infection, showing an increase in ScaA
371 labelling and a decrease in ScaC labelling. * p-value ≤ 0.05, ** p-value ≤ 0.01, *** p-value ≤ 0.001.
372

373 **Fig. 4: Both IB and EB populations are infectious but differ in physical stability and**
374 **mechanism of entry into cells.**

375 A. IB and EB Ot were isolated from infected L929 cells five days post-infection and grown in fresh
376 L929 cells in a 24-well plate. The number of intracellular bacteria was then quantified at 3, 24, 96,
377 and 168 hours post-infection using qPCR against *tsa47,* a single copy Ot gene. Doubling times
378 of IB and EB Ot were similar. B. IB and EB were exposed to physical stress using a bead mill for
379 one or two min; growth was quantified as in 4A. The bead mill did not affect the growth rate of IB
380 Ot but reduced that of EB Ot in an exposure-dependent manner. C. IB and EB were exposed to
381 osmotic shock by suspending the bacteria in water for five min and then growing them in fresh
382 L929 cells. Bacterial copy number after seven days was quantified by qPCR. EB was more
383 susceptible to osmotic shock than IB Ot, as shown by a more significant decrease in bacterial
384 number. D. Quantification of the effect of endocytosis inhibitors on entry of IB and EB Ot. IB and
385 EB were isolated from L929 cells five days post-infection and then seeded onto fresh HUVEC
386 cells that had been treated with inhibitors of clathrin-mediated endocytosis (dynasore) or

387 macropinocytosis (amiloride). Cells were fixed three hours post-infection. Dynasore inhibits entry
388 of IB but not EB, indicating that clathrin-mediated endocytosis is the major mode of entry of this
389 population, whilst amiloride strongly inhibited EB and, to a lesser extent, IB. This observation
390 points to a role for macropinocytosis in EB's entry into mammalian cells. Confocal microscopy
391 images shown in E. Red = actin (phalloidin), blue = hoescht (DNA), green = Ot (anti-TSA56
392 antibody). Scale bar = 10 μm. Similar results were found in L929 cells (Supp. Fig. 6).
393
394 **Fig.5: An overview of the infection cycle of Ot, showing differentiation between IB and EB**
395 **forms.**
396 IB replicate in a micro-colony adjacent to the nucleus where they are elongated in shape and
397 translationally active. Bacteria move to the cell's edge and transition to an EB form that is round
398 and translationally inactive. Created with BioRender.com B. Table summarizing the differences
399 between IB and EB forms of Ot.
400

401 **Methods**

402

403 **Cell culture, bacterial propagation and quantification, and reagents**

404 Proteomics and qRT-PCR experiments were performed using the mouse fibroblast cell line L929
405 kindly provided by Dr. Blacksell at the Mahidol Oxford Tropical Medicine Research Unit, Bangkok,
406 Thailand. For all other experiments, we used L929 cells purchased from ATCC (ATCC CCL-1) or
407 Primary Human Umbilical Vein Endothelial Cells (HUVEC), also from ATCC (ATCC PCS-100-
408 010). We cultured cells in either DMEM (L929) or Large Vessel Endothelial Supplement (LVES,
409 HUVEC) supplemented with 10% FBS (Gibco 16140071) at 37ºC and a 5% CO_2 atmosphere.
410 The Karp-like clinical isolate strain of *Orientia tsutsugamushi* UT76[22] was used throughout the
411 study. For routine propagation, bacteria were grown in 25- or 75-cm^2 culture flasks, as described
412 previously[12]. We extracted DNA using alkaline lysis buffer[12], and then assessed bacterial
413 quantities by determining genome copy numbers relative to a standard curve. We used a
414 primer/probe set to amplify the single copy gene *tsa47* (tsa47F 5'-
415 TCCAGAATTAAATGAGAATTTAGGAC-3', tsa47R 5'-TTAGTAATTACATCTCCAGGAGCAA-3',
416 tsa47probe 5'-[6FAM]TTCCACATTGTGCTGCAGATCCTTC[TAM]-3') or the 16S gene
417 (Rick16SF 5'- GCTACACGCGTGCTACAATGG-3', Rick16SR 5'-
418 TGTGTACAAGGCCCGAGAACG-3', Rick16Sprobe 5'-[6FAM]
419 ATCGCTAGTAATCGCGGATCAGCATGCC [TAM]-3'). For drug inhibition assays, dynasore
420 (Sigma D7693) and amiloride (Sigma A3085) were added to L929 or HUVEC cells 1 hour before
421 infection with Ot.

422

423 **Fluorescence microscopy**

424 **Immunofluorescence labelling and confocal microscopy.** Following fixation, cells were
425 permeabilized by incubation in 0.5% Triton X-100 for 30 min on ice followed by blocking in 1XPBS
426 (pH7.4) containing either 1 mg/ml BSA or sera (diluted 1:20) matching the labeled antibody's host,

427 for 30 min at room temperature. Incubations with primary antibodies took place for 1 hour at 37ºC.
428 These studies were conducted using in-house-generated antibodies (*i.e.*, rat monoclonal antibody
429 against TSA56 diluted 1:200; rabbit polyclonal antibody against Ot ScaC diluted 1:200) or
430 commercial products (*i.e.*, MA1-164, a Thermo Scientific monoclonal mouse antibody against
431 LAMP1 diluted 1:200). The fixed cells were washed twice with PBS-BSA and were then incubated
432 with appropriate secondary antibodies (1:1000 dilutions) for 30 min at 37ºC in the dark. We used
433 the following secondary antibodies: goat anti-mouse IgG superclonal Alexa Fluor 647 conjugate
434 (Thermo Fisher A28180), goat anti-rat Alexa Fluor 488 (Thermo Fisher A11006), and goat anti-
435 rabbit Alexa Fluor 594 (Thermo Fisher A11012). The nuclear stain Hoechst (1:1000 dilution) was
436 supplemented to incubations with secondary antibodies. Phalloidin Alexa Fluor 594 (1:200,
437 ThermoFisher Scientific A12381) was used to detect host actin. The cells were washed with 1X
438 PBS before supplementation of mounting medium [20 mM Tris (pH 8.0); 0.5% N-propyl-gallate;
439 90% glycerol]. Imaging was performed using a Zeiss Observer Z1 LSM700 confocal microscope
440 with an HBO 100 illuminating system equipped with a 63x/1.4 Plan-APOCHROMAT objective lens
441 (Carl Zeiss, Germany) and 405 nm, 488 nm, and 555 nm laser lines. In some cases, we used a
442 Leica TCS SP8 confocal microscope (Leica Microsystems, Germany) equipped with a 63x/1.4
443 Plan-APOCHROMAT oil objective lens with a 1.4-mm working distance and 405 nm, 488 nm, 552
444 nm, and 638 nm laser lines.
445 Fluorescence intensity measurements were performed manually using Fiji ImageJ software. 30
446 (Fig. 3C) or 100 (Fig. 1G); individual bacteria were quantified by measuring the brightest pixel
447 intensity within the bacterial area. Images from individual experiments were acquired under
448 identical laser intensity and acquisition conditions. Length and width measurements were
449 performed manually using Fiji Image J software.
450
451 **STORM imaging and analysis**

452 We acquired 3D-STORM data using a homebuilt multi-color Total Internal Reflection
453 Fluorescence (TIRF) microscope[26] that is based on an inverted microscope (Nikon, Ti-E), a high
454 NA objective (Nikon, CFI-Apo 100X, NA 1.49), a 405 nm photoactivation laser (Coherent, OBIS
455 405 LX 100mW), a 488 nm excitation laser (MPB, 2RU-VFL-P-20000642-B1R), and an EMCCD
456 camera (Andor, iXon Ultra-888). Samples immunolabelled with Alexa 488 were mounted on the
457 microscope, transferred to STORM buffer [OxyFluor (Oxyrase), 50 mM BME (Sigma), 2.5 mM
458 COT (Sigma)], and illuminated with a strong (488 nm) laser to record single-molecule
459 fluorescence blinking events at a frame rate of 25 Hz. Illumination at 405 nm was intercalated with
460 pulsed 488nm excitation to enhance photoactivation of Alexa 488 without exacerbating
461 background signal. A cylindrical lens (Thorlabs, LJ1516RM-A) was placed in front of the camera
462 to determine the z-coordinates of fluorescent molecules through the elongated point spread
463 function (PSF) methods[27]. Each STORM image was reconstructed from single-molecule
464 localization data obtained by analysing 30,000 frames with custom Matlab codes. Briefly, bright
465 single fluorescence spots were identified by thresholding methods, and their 3-D coordinates were
466 determined by 2-D elliptical Gaussian fitting along with a pre-calibrated conversion table between
467 eccentricity and z-coordinate. Focus drift was actively stabilized with Perfect Focus System
468 (Nikon) while acquiring the data, whereas xy-drift was post-corrected using a redundant cross-
469 correlation algorithm[28]. Each localization event was represented as a 2-D Gaussian of 20 nm
470 standard deviation in STORM images. For the analysis of bacterial morphology, we selected cells
471 that showed clear cell boundary, manually adjusted the z-coordinate to locate the cell midplane,
472 and measured long- and short- axes length.
473

474 **Click labelling.** Our metabolic click-labelling was based on the Click-iT HPG Alexa Fluor protein
475 Synthesis Assay Kit (Click-iT HPG Alexa Fluor Protein Synthesis Assay Kit, ThermoFisher
476 C10428) strategy. To incorporate L-homopropargylglycine (HPG), we incubated infected cells

477 with minimal medium (Dulbecco's Modified Eagle Medium, DMEM, ThermoFisher 21013) lacking
478 L-methionine and containing 25 µM HPG, for 30 min at 37ºC. Labelled bacteria were washed
479 twice with PBS containing 1mg/ml BSA, fixed with 1% formaldehyde, and subsequently
480 permeabilized with 0.5% Triton X-100 for 20 min on ice. After further washing with PBS containing
481 1 mg/ml BSA, we supplemented the Click-iT reaction cocktail (Click-iT HPG Alexa Fluor Protein
482 Synthesis Assay Kit, ThermoFisher C10428) and incubated the cells for 30 min at room
483 temperature in a light protected environment. The Azide dye (Alexa Fluor 488) was used at a final
484 concentration of 5 µM. Following completion of the click reaction, the cells were subjected to
485 immunofluorescence labelling and imaging as above.
486
487 **Gene expression analysis by RT-qPCR**
488 L929 cells were transfected with *Orientia tsutsugamushi* UT76 using multiple MOIs (*i.e.*, 672:1,
489 300:1, 560:1, 333:1, and 267:1). Infected cells were harvested four days after transfection and
490 were stored in RNAProtect Bacteria Reagent (Qiagen 76506) at -80ºC. Total RNA was extracted
491 using the Qiagen RNeasy Plus kit (Qiagen 74136) according to the manufacturer's instructions.
492 One µg of total RNA was incubated with DNaseI (Thermo Fisher Scientific, AM2238) for 16 h at
493 37ºC, and the samples were then reverse-transcribed using the iScript reverse transcription
494 supermix (Biorad 170–8841) and random primers. Controls lacking reverse transcriptase
495 demonstrated that the RNA sample used for cDNA synthesis was not contaminated with genomic
496 DNA. The resulting cDNA was then used as template for qPCR using primers for *spoT, rpoH,*
497 *obgE, yccA, nuoB, dapA, curA, sodB, trxB, tsa56, and scaA.* RT-qPCR was performed using
498 SYBR green qPCR mix (Biotools 10.609). Expression levels were normalized relative to the
499 housekeeping genes *16sRNA, ank12_1 and mipZ*.
500

Primer name	Primer sequences (5’ to 3’)

spoT forward	GGCAGACATAAAGCACCTTAC
spoT reverse	GAAATCTTGAAAGCTGCCAGG
rpoH forward	CTGCCGAAGAGGAATATATGC
rpoH reverse	CCCCTCGGAAACTAAATCAAC
obgE forward	GCACAAAATGGTAGAGCTGG
obgE reverse	GAATCACCAATCTCACCTACAG
yccA forward	GCTATTGCAGGAACCGCTAC
yccA reverse	CTGAAAGCGACATGCCTACA
nuoB forward	GGGCTAGAACACGCTCGTTA
nuoB reverse	GCACAGCTACCCATTGATATC
dapA forward	GGTAGAACATTAGTGATTGCTGG
dapA reverse	GCGTCTTTGATTGCTACTATCC
curA forward	AGTAGGGCAACGAGTTGGC
curA reverse	CAACAGCGCTACTAGCAGC
sodB forward	GTAGTGGTTGGGTCTGGTTG
sodB reverse	GTTCAGCAAATCGCCAATTTG
trxB forward	GATATGCACTGGTGCTCAAG
trxB reverse	CACCTCCTACAACAACTACTC
tsa56 forward	TGCCCAACAAGAAGAAGATG
tsa56 reverse	TTTAACTTGGCCGACAATCA
scaA forward	TAGTGAAAGGGGACGATTGC
scaA reverse	ATCCGACAAGTTAGGCATGG
*16s*RNA forward	CGGTGAATACGTTCTCGGG
*16s*RNA reverse	GAGGTAATCCAGCCGCAGG
ank12_1 forward	GATAGCAGAGGTTGTACACCG

ank12_1 reverse	CTGATTTGTTAGGCTGCCTGC
mipZ forward	GTGGTGCAGGTAAGACTACTGTTG
mipZ reverse	GTGAATGCTGACGTGAATCAG

501

502 **Proteomics sample preparation**

503 We used *Orientia tsutsugamushi* strain UT76 to infect L929 mouse fibroblasts at a 410:1 MOI in
504 six independent culture flasks. We replaced the culture medium at one-day post-infection (dpi) to
505 remove bacteria that failed to enter the host. Intracellular and extracellular bacteria were isolated
506 at four dpi; two separate flasks were harvested as one replicate, yielding a total of three replicates.
507 L929 cells were grown in 75-cm^2 plastic flasks at 37°C in a 5% CO_2 atmosphere, using DMEM
508 media (Gibco 11965092) supplemented with 10% FBS (Sigma-Aldrich F7524). At four dpi, the
509 media were transferred to 50-ml conical tubes for extracellular bacteria isolation. Culture flasks
510 were rinsed with 15 ml of PBS, and cells were scraped using two ml of fresh media per flask. The
511 lysates were transferred to two-ml Safe-lock tubes and homogenized for three minutes using a
512 Bullet blender® homogenizer (Next Advance #BBY24M) using speed control setting at 8. Host cell
513 debris was removed by centrifugation at 300xg for three minutes; we then harvested intracellular
514 bacteria by an additional three-minute centrifugation at 20,000xg. Before isolation of extracellular
515 bacteria, we removed detached host cells through a pre-spin step (1,000 xg, 5 min, 4ºC).
516 Following transfer of supernatants to new conical tubes, we harvested extracellular bacteria by
517 centrifugation at 3000xg for 20 minutes at 4ºC. Intracellular and extracellular bacteria were
518 washed with 0.3 M sucrose three times, resuspended in PBS, and lysed with 1% Triton X-100 for
519 30 minutes at 4ºC. Bacterial proteins were precipitated by addition of 80% ice-cold acetone and
520 overnight incubation at -20ºC. Protein pellets were washed in acetone twice to remove residual
521 Triton X-100 by centrifugation at 15,000xg for 10 min. Briefly dried protein extracts were then
522 dissolved in 100 µl of 50% trifluoroethanol in 100 mM TEAB buffer. The samples were reduced
523 by treatment with 20 mM TCEP for 20 minutes at 55ºC, alkylated in 55 mM CAA at room

524 temperature in the dark, and digested with LysC (LysC: protein ratio=1:50) overnight at 37ºC and,
525 subsequently, with trypsin (trypsin: protein ratio=1:100), also overnight at 37ºC. Samples were
526 acidified with TFA to 1% final concentration and centrifuged to remove insoluble materials.
527 Trypsinized samples were desalted using an Oasis® HLB 1cc cartridge (Waters). Briefly, following
528 cartridge activation with 500 µl of 100% acetonitrile and equilibration with 500 µl of 0.5% acetic
529 acid, we loaded samples and then washed the cartridge with 1 ml MS-grade water. Peptides were
530 eluted with 500 µl of 80% acetonitrile in 0.5% acetic acid, then transferred to low-binding
531 microtubes, and dried using a SpeedVac. We estimated peptide content using 5% of each
532 sample. Briefly, individual aliquots in 1 µl of MS-grade water were supplemented with 4 µl of 1%
533 (v/v) acetonitrile containing 0.06% (v/v) trifluoroacetic acid and 0.5% (v/v) acetic acid, transferred
534 to a 96-well autosampler plate, and then injected (3 µl) into an Orbitrap Fusion™ Mass
535 Spectrometer. The remaining 95% of each sample (19 µl in MS-grade water) was mixed with 20
536 µl of 10 mM ammonium formate (pH 10) and centrifuged at 20,000xg for 3 min to eliminate
537 insoluble components. Each peptide sample was then fractionated through a step-wise desalting
538 process on C18 stage tips using 10%, 15%, 25%, and 50% acetonitrile in 10 mM ammonium
539 formate (pH 10). Fractionated samples were washed with 60% acetonitrile containing 0.1% formic
540 acid twice to eliminate residual ammonium formate by evaporation before tandem MS analysis.
541
542 **LC-MS/MS**
543 Dried samples were resuspended in 2% (v/v) acetonitrile containing 0.06% (v/v) trifluoroacetic
544 acid and 0.5% (v/v) acetic acid, and loaded onto an autosampler plate. Online chromatography
545 was performed in an EASY-nLC 1000 (ThermoScientific) instrument using a one-column setup
546 and 0.1% formic acid in water / 0.1% formic acid in acetonitrile as mobile phases. The samples
547 were injected and separated on a reversed-phase C18 analytical column (EASY-Spray LC
548 Column, 75 µm inner diameter × 50 cm, 2 µm particle size; ThermoScientific) maintained at 50°C
549 and using a 2-23% (v/v) acetonitrile gradient over 60 min, followed by an increase to 50% over

550 the next 20 min, and to 90% over 5 min. The final mixture was maintained on the column for 5
551 min to elute all remaining peptides. Total run duration for each sample was 90 min at a constant
552 flow rate of 300 nl/min.
553 Data were acquired using an Orbitrap Fusion Lumos™ mass spectrometer (ThermoScientific)
554 using the instrument's data-dependent mode. Samples were ionized using 2.5 kV and 300°C at
555 the nanospray source; positively-charged precursor MS1 signals were detected using an Orbitrap
556 analyser set to 60,000 resolution, automatic gain control (AGC) target of 400,000 ions, and
557 maximum injection time (IT) of 50 ms. Precursors with charges 2-7 and having the highest ion
558 counts in each MS1 scan were further fragmented using collision-induced dissociation (CID) at
559 35% normalized collision energy. MS2 signals were analysed by ion trap at an AGC of 15,000
560 and maximum IT of 50 ms. Precursors used for MS2 scans were excluded for 90 s to avoid re-
561 sampling of high abundance peptides. The MS1–MS2 cycles were repeated every 3 s until
562 completion of the run.
563
564 **Proteomic data analysis**
565 Proteins were identified using Proteome Discoverer™ (v2.3, Thermo Scientific). Raw mass
566 spectra were searched against *Orientia tsutsugamushi* primary protein sequences derived from
567 complete genome data for the UT76 strain. Mouse whole proteome sequences were obtained
568 from Uniprot and included as background. Carbamidomethylation on Cys was set as a fixed
569 modification; deamidation of asparagine and glutamine, acetylation on protein N termini, and
570 methionine oxidation were set as dynamic modifications for the search. Trypsin/P was set as the
571 digestion enzyme and was allowed up to three missed cleavage sites. Precursors and fragments
572 were accepted if they had a mass error within 10 ppm and 0.8 Da, respectively. Peptides were
573 matched to spectra at a false discovery rate (FDR) of 1% against the decoy database.
574 For label-free quantitation (LFQ), features were extracted from the raw data files using the Minora
575 Feature Detector processing workflow node on Proteome Discoverer. Chromatographic feature-

576 matching was performed with a tolerance of 10 min to align the retention times and enable
577 quantitation of the precursors. No pre-normalization was performed using the Proteome
578 Discoverer workflow, and raw results were manually normalized using the Median normalization
579 method. A protein was classified as detected if at least two peptides were detected in a minimum
580 of two biological replicates; the mean LFQ across the three replicates was used for further
581 analyses.
582
583 **Immunoblot analyses**
584 L929 and HUVEC cells were grown in 24-well plates and infected with Ot UT76 at an MOI of 12:1.
585 Non-infectious bacteria were removed by replacing the media 24 hours post-infection. EB and IB
586 populations were prepared four-seven days post-infection. EB was prepared by transferring the
587 cell supernatant to an Eppendorf tube, pelleting at 16,873xg, then resuspending in 100 µl PBS
588 containing 1x protease inhibitor cocktail (ThermoFisher 78425). For TSA56 immunoblots,
589 samples were prepared in the presence of 1 mM iodoacetamide (Sigma-Aldrich catalog number
590 I6125). IB was prepared by removing adherent cells using trypsinization, spinning the cell pellet,
591 and resuspending it in PBS supplemented with protease inhibitors; host cells were lysed using a
592 bead mill for 1 minute. Host cell debris was removed by centrifugation at 500xg for 5 min; the
593 supernatant was transferred to a clean tube, spun at 16,873xg for 5 minutes, and resuspended
594 in 100 µl PBS supplemented with protease inhibitors. Bacterial copy number was quantified by
595 qPCR using *tsa47* primers, as described above. IB and EB samples were diluted to ensure equal
596 loading of bacterial cells on gels. Samples were diluted in 5X SDS loading buffer with and without
597 ß-mercaptoethanol and heated at 95ºC for 5 min. Samples were subjected to electrophoresis on
598 a 4-20% gradient gel (Bio-Rad 4561094) and then transferred to a nitrocellulose membrane.
599 Following blocking in PBST containing 5% BSA for 30 min, we incubated the blots with primary
600 antibody (1:1,000) in PBST-BSA overnight at 4ºC. Membranes were washed and incubated with
601 secondary antibody (1:10,000) conjugated to IRDYE 680RD or IRDYE 800CW (LI-COR

602 Biosciences) in PBST-BSA for 1 hour at room temperature. Membranes were washed, and
603 immunoreactive proteins were visualized using a LiCor Odyssey CLX imager.
604
605 **Quantification of genome copy number per cell**
606 The genome copy number per cell was calculated by determining the number of bacterial genome
607 copies in a sample of purified EB and IB Ot, using *tsa47* qPCR, and dividing by the number of
608 bacterial cells in the same sample, as measured by confocal microscopy. Three µl of purified
609 bacteria were spread evenly across a well of a multi-well slide, dried, and labelled for
610 immunofluorescence microscopy using TSA56, as described above. The bacteria in a selected
611 field were manually counted to determine the number of bacterial cells in the sample.
612
613 **Quantification of relative peptidoglycan levels using NOD1 reporter assay**
614 HEK-Blue hNOD1 cells (Invitrogen, hkb-hnod1, USA) were grown in DMEM containing 4.5 g/l
615 glucose, 10% heat-inactivated FBS, 100 U/ml penicillin, 100 mg/ml streptomycin, 100 mg/ml
616 Normocin, 2 mM L-glutamine, and the selective antibiotics blasticidin (30 µg/ml) and Zeocin (100
617 µg/ml). The cells were seeded on clear-bottom black 96-well plates (Corning 29444-008) 2 days
618 before treatment. Bacterial aliquots from stocks kept in sucrose phosphate glutamine (SPG) at -
619 80°C were heat-inactivated at 90°C for 30 minutes before supplementation to host cells. These
620 studies were carried out in triplicate. After two days, growth media were replaced with HEK-blue
621 detection media (Invivogen, hb-det2) for SEAP assessment. The plates were further incubated
622 for six hours at 37°C in a 5% CO_2 atmosphere and then analyzed spectrophotometrically (Synergy
623 H1, Biotek) at 640 nm. Results were analyzed by GraphPad Prism (GraphPad Software, San
624 Diego California USA), and a t-test was performed to compare bacterial SEAP levels to positive
625 control iE-DAP (γ-D-Glu-mDAP) at 10 µg/ml.
626
627 **Growth curve measurements and bead mill treatment**

628 To determine the growth rate of IB and EB Ot from frozen stock were first grown in two T25
629 flasks containing a monolayer of L929 cells. At 6 days post infection, IB and EB were prepared
630 and used to inoculate fresh L929 cells and the subsequent bacterial growth was
631 measured. **EB isolation** – the supernatant portion of the culture consisting of EB was
632 transferred to a 50-mL centrifuge tube (Corning, catalog no. 430828) and subjected to a first
633 centrifugation to remove any host cells at 1,500 rcf for 5 minutes. The supernatant was then
634 transferred into a new 50-ml tube and centrifuged at 3,220 rcf for 20 minutes to obtain an EB
635 pellet which was resuspended in the fresh media and ready for the next step. **IB isolation** –
636 fresh media was added directly to the culture flasks containing infected cells and these
637 were disassociated from the adherent surface by using a cell scraper (Corning Falcon,
638 catalog no. 353089). The infected cell suspension was then pipetted into a sterile 2-mL
639 microcentrifuge tube. (Eppendorf, catalog no. 022363352) pre-filled with sterile 0.1-0.15 mm
640 diameter glass beads (Biospec, catalog no. 11079101) before introduced to VWR® Bead Mill
641 Homogenizer (VWR, catalog no. 10158-558) at speed 5 for 1 minutes to break the host cells.
642 Subsequently, the purified IB in the supernatant was separated from host cells debris and
643 glass beads by transferring the supernatant into a new 2-mL microcentrifuge tube and
644 spinning at 300 rcf for 5 minutes. The bacterial concentration in both EB and IB suspension
645 was quantified by qPCR as described above, and EB and IB Ot was infected onto a fresh
646 monolayer of L929 cells in 12-well plates (Thermo Scientific, catalog no. 150628). Bacteria
647 were added at 2.83E+04 bacterial copies/well which corresponds to an MOI of ~1:10. The
648 number of intracellular bacteria was then measured at 3, 24, 96 and 168 hours post infection
649 by *tsa47* qPCR. **Physical stress induced by bead mill** – IB and EB isolation and infection
650 were performed as described above and then exposed to physical stress with 1 or 2 minutes
651 agitation in the bead mill. Bacteria were then infected onto L929 cells at a concentration of
652 1.00E+06 copies/well (MOI = 2:1). The quantity of intracellular bacteria was then determined

653 at 3, 24, 96, 120, 144 and 168 hours post infection by qPCR. **Osmotic stress induced by**
654 **water treatment.** Quantification of the effect of osmotic shock on Ot viability was performed
655 in the same way as for physical stress except purified bacteria were resuspended in pure
656 water for 5 minutes prior to infecting host cells. Bacterial copy number after 7 days was
657 quantified by qPCR.
658
659

Acknowledgements and Funding

We thank each laboratory member for valuable discussions and support. We are grateful to the following people for providing helpful feedback and insightful comments related to the project and the manuscript: Jonathan Dworkin from Columbia University, Dave Dubnau from PHRI, and Diana Stafforini from Life Science Editors.

This work was funded by a Royal Society Dorothy Hodgkin Research Fellowship (JS) (DH140154), a Newton Fund MRC-NSTDA grant (YJ) (MR/N012380/1), and National Institute of Health/National Institute of Allergy and Infectious Diseases grants (R21AI144385 and R56AI148645).

671 **References**

672

673 1 Taylor, A., Paris, D. & Newton, P. A Systematic Review of Mortality from Untreated
674 Scrub Typhus (Orientia tsutsugamushi). *PLoS Negl Trop Dis* **9**, e0003971,
675 doi:10.1371/journal.pntd.0003971 (2015).
676 2 Luce-Fedrow, A. *et al.* A Review of Scrub Typhus (Orientia tsutsugamushi and Related
677 Organisms): Then, Now, and Tomorrow. *Tropical Medicine and Infectious Disease* **3**, 8,
678 doi:10.3390/tropicalmed3010008 (2018).
679 3 McClure, E. *et al.* Engineering of obligate intracellular bacteria: progress, challenges and
680 paradigms. *Nat Rev Microbiol*, doi:10.1038/nrmicro.2017.59 (2017).
681 4 Salje, J. Cells within cells: Rickettsiales and the obligate intracellular bacterial lifestyle.
682 *Nat Rev Microbiol*, doi:10.1038/s41579-020-00507-2 (2021).
683 5 Rikihisa, Y. & Ito, S. Localization of electron-dense tracers during entry of Rickettsia
684 tsutsugamushi into polymorphonuclear leukocytes. *Infect Immun* **30**, 231-243 (1980).
685 6 Lee, J. *et al.* Fibronectin facilitates the invasion of Orientia tsutsugamushi into host cells
686 through interaction with a 56-kDa type-specific antigen. *J Infect Dis* **198**, 250-257,
687 doi:10.1086/589284 (2008).
688 7 Ha, N., Cho, N., Kim, Y., Choi, M. & Kim, I. An autotransporter protein from Orientia
689 tsutsugamushi mediates adherence to nonphagocytic host cells. *Infect Immun* **79**, 1718-
690 1727, doi:10.1128/IAI.01239-10 (2011).
691 8 Ha, N. *et al.* Immunization with an Autotransporter Protein of Orientia tsutsugamushi
692 Provides Protective Immunity against Scrub Typhus. *PLoS Negl Trop Dis* **9**, e0003585,
693 doi:10.1371/journal.pntd.0003585 (2015).
694 9 Chu, H. *et al.* Exploitation of the endocytic pathway by Orientia tsutsugamushi in
695 nonprofessional phagocytes. *Infect Immun* **74**, 4246-4253, doi:10.1128/IAI.01620-05
696 (2006).
697 10 Kim, H., Choi, M. & Kim, I. Role of Syndecan-4 in the cellular invasion of Orientia
698 tsutsugamushi. *Microb Pathog* **36**, 219-225, doi:10.1016/j.micpath.2003.12.005 (2004).
699 11 Cho, B., Cho, N., Seong, S., Choi, M. & Kim, I. Intracellular invasion by Orientia
700 tsutsugamushi is mediated by integrin signaling and actin cytoskeleton rearrangements.
701 *Infect Immun* **78**, 1915-1923, doi:10.1128/IAI.01316-09 (2010).
702 12 Giengkam, S. *et al.* Improved Quantification, Propagation, Purification and Storage of
703 the Obligate Intracellular Human Pathogen Orientia tsutsugamushi. *PLoS Negl Trop Dis*
704 **9**, e0004009, doi:10.1371/journal.pntd.0004009 (2015).
705 13 Atwal, S. *et al.* Evidence for a peptidoglycan-like structure in Orientia tsutsugamushi.
706 *Mol Microbiol* **105**, 440-452, doi:10.1111/mmi.13709 (2017).
707 14 Min, C. *et al.* Genome-based construction of the metabolic pathways of Orientia
708 tsutsugamushi and comparative analysis within the Rickettsiales order. *Comp Funct*
709 *Genomics* **2008**, 623145, doi:10.1155/2008/623145 (2008).
710 15 Atwal, S. *et al.* Clickable methionine as a universal probe for labelling intracellular
711 bacteria. *J Microbiol Methods* **169**, 105812, doi:10.1016/j.mimet.2019.105812 (2020).

712 16 Rikihisa, Y. Anaplasma phagocytophilum and Ehrlichia chaffeensis: subversive
713 manipulators of host cells. *Nat Rev Microbiol* **8**, 328-339, doi:10.1038/nrmicro2318
714 (2010).
715 17 Elwell, C., Mirrashidi, K. & Engel, J. Chlamydia cell biology and pathogenesis. *Nat Rev*
716 *Microbiol* **14**, 385-400, doi:10.1038/nrmicro.2016.30 (2016).
717 18 Eldin, C. *et al.* From Q Fever to Coxiella burnetii Infection: a Paradigm Change. *Clin*
718 *Microbiol Rev* **30**, 115-190, doi:10.1128/CMR.00045-16 (2017).
719 19 Otten, C., Brilli, M., Vollmer, W., Viollier, P. & Salje, J. Peptidoglycan in obligate
720 intracellular bacteria. *Mol Microbiol* **107**, 142-163, doi:10.1111/mmi.13880 (2018).
721 20 Jacquier, N., Frandi, A., Pillonel, T., Viollier, P. & Greub, G. Cell wall precursors are
722 required to organize the chlamydial division septum. *Nat Commun* **5**, 3578,
723 doi:10.1038/ncomms4578 (2014).
724 21 Irving, S. E., Choudhury, N. R. & Corrigan, R. M. The stringent response and physiological
725 roles of (pp)pGpp in bacteria. *Nat Rev Microbiol*, doi:10.1038/s41579-020-00470-y
726 (2020).
727 22 Batty EM, C. S., Blacksell SB, Richards A, Paris D, Bowden R, Chan C, Lachumanan R, Day
728 N, Donnelly P, Chen SL, Salje J. Long-read whole genome sequencing and comparative
729 analysis of six strains of the human pathogen Orientia tsutsugamushi. *Plos Negl Trop Dis*
730 (2018).
731 23 Mika-Gospodorz, B. *et al.* Dual RNA-seq of Orientia tsutsugamushi informs on host-
732 pathogen interactions for this neglected intracellular human pathogen. *Nat Commun* **11**,
733 3363, doi:10.1038/s41467-020-17094-8 (2020).
734 24 Joshi, K. K. & Chien, P. Regulated Proteolysis in Bacteria: Caulobacter. *Annu Rev Genet*
735 **50**, 423-445, doi:10.1146/annurev-genet-120215-035235 (2016).
736 25 Lamason, R. *et al.* Rickettsia Sca4 Reduces Vinculin-Mediated Intercellular Tension to
737 Promote Spread. *Cell* **167**, 670-683.e610, doi:10.1016/j.cell.2016.09.023 (2016).
738 26 Lee, S. Optimal integration of wide field illumination and holographic optical tweezers
739 for multimodal microscopy with ultimate flexibility and versatility. *Opt Express* **26**, 8049-
740 8058, doi:10.1364/OE.26.008049 (2018).
741 27 Huang, B., Wang, W., Bates, M. & Zhuang, X. Three-dimensional super-resolution
742 imaging by stochastic optical reconstruction microscopy. *Science* **319**, 810-813,
743 doi:10.1126/science.1153529 (2008).
744 28 Wang, Y. *et al.* Localization events-based sample drift correction for localization
745 microscopy with redundant cross-correlation algorithm. *Opt Express* **22**, 15982-15991,
746 doi:10.1364/OE.22.015982 (2014).
747

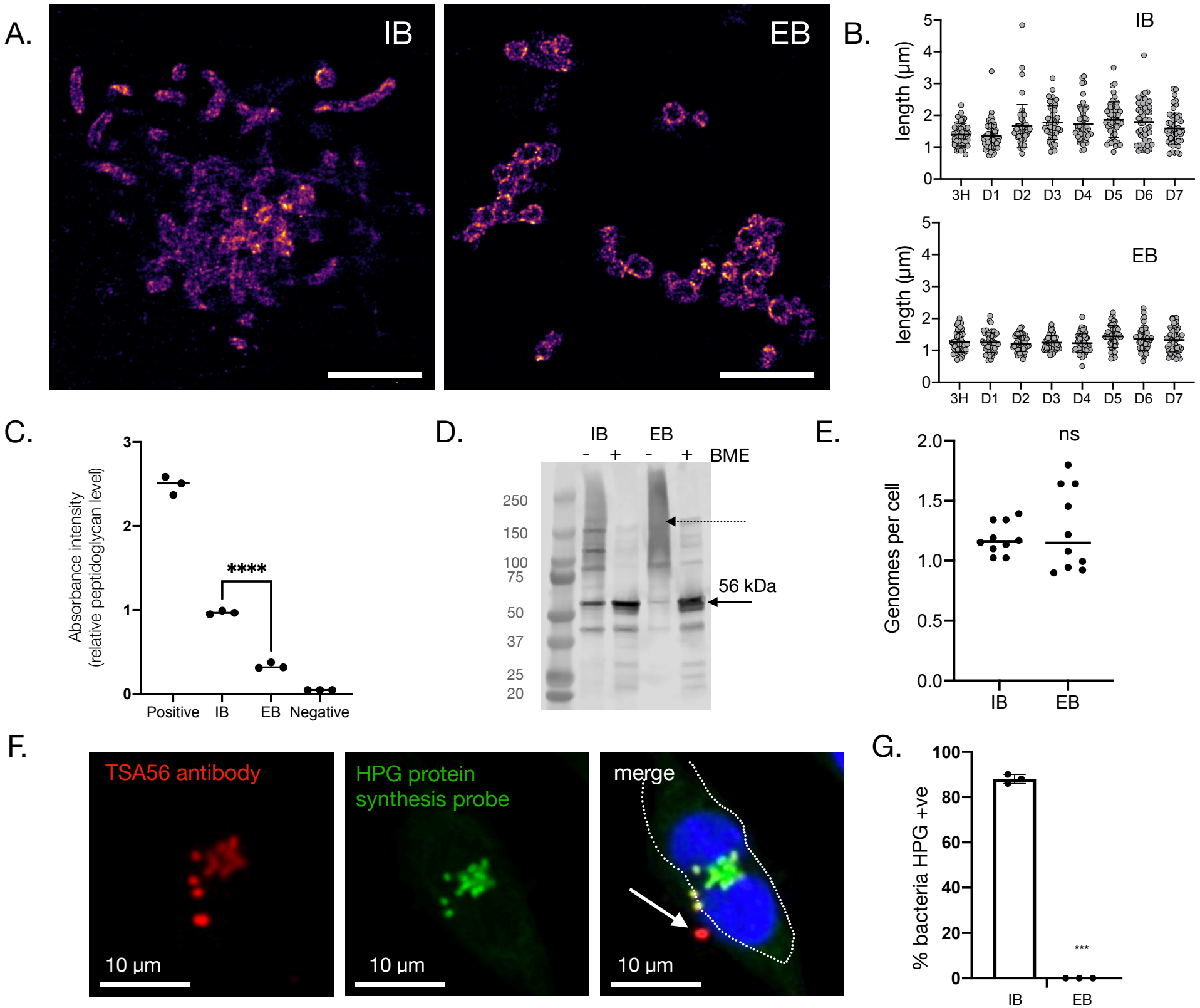

Fig. 1: Intracellular and extracellular forms of Ot are physically and metabolically distinct.
A. STORM images of IB and EB Ot in L929 cells. Bacteria were labelled with a monoclonal antibody against surface protein TSA56. Additional images are provided in Supp. Fig. 1. B. Length quantification of individual IB and EB Ot as imaged by STORM. C. Quantification of relative peptidoglycan levels through activation of NOD1 reporter cells, as measured by secreted alkaline phosphatase activity. EB Ot induced less activation than IB, indicating lower levels of peptidoglycan. Identical amounts of IB and EB Ot were used, and biological triplicates are shown. D. Immunoblot showing the formation of disulfide cross-linked aggregates of the surface protein TSA56, observed in the absence of the reducing agent beta-mercaptoethanol (BME). This effect was stronger in EB compared with IB Ot. The expected molecular weight of TSA56 (56 kDa) is indicated with an arrow, and a dashed arrow depicts higher-order aggregates. E. Genome copy number per cell as measured by qPCR; bacterial cell number was determined by immunofluorescence microscopy. Quantification of 10 individual imaging fields is shown. F. Confocal microscopy image of an L929 cell infected with Ot and labelled with the clickable methionine analog homopropargylglycine (HPG, green) and an antibody against surface protein TSA56 (red). The host cell outline is showed by a dashed line, and an arrow indicates a metabolically inactive bacterium located outside the host cell. G. Quantification of metabolic activity, as measured by a detectable HPG signal, in IB and EB Ot. L929 cells were infected with Ot for five days, fixed, and labelled with TSA56 and HPG. One-hundred bacteria inside (IB) and outside cells (EB) were counted and scored as being HPG-positive or -negative. The percentage of HPG-positive IB and EB Ot, based on individual values from three independent replicates. Statistical significance (t-test) was determined using Graphpad Prism software. p-value *** ≤ 0.001.

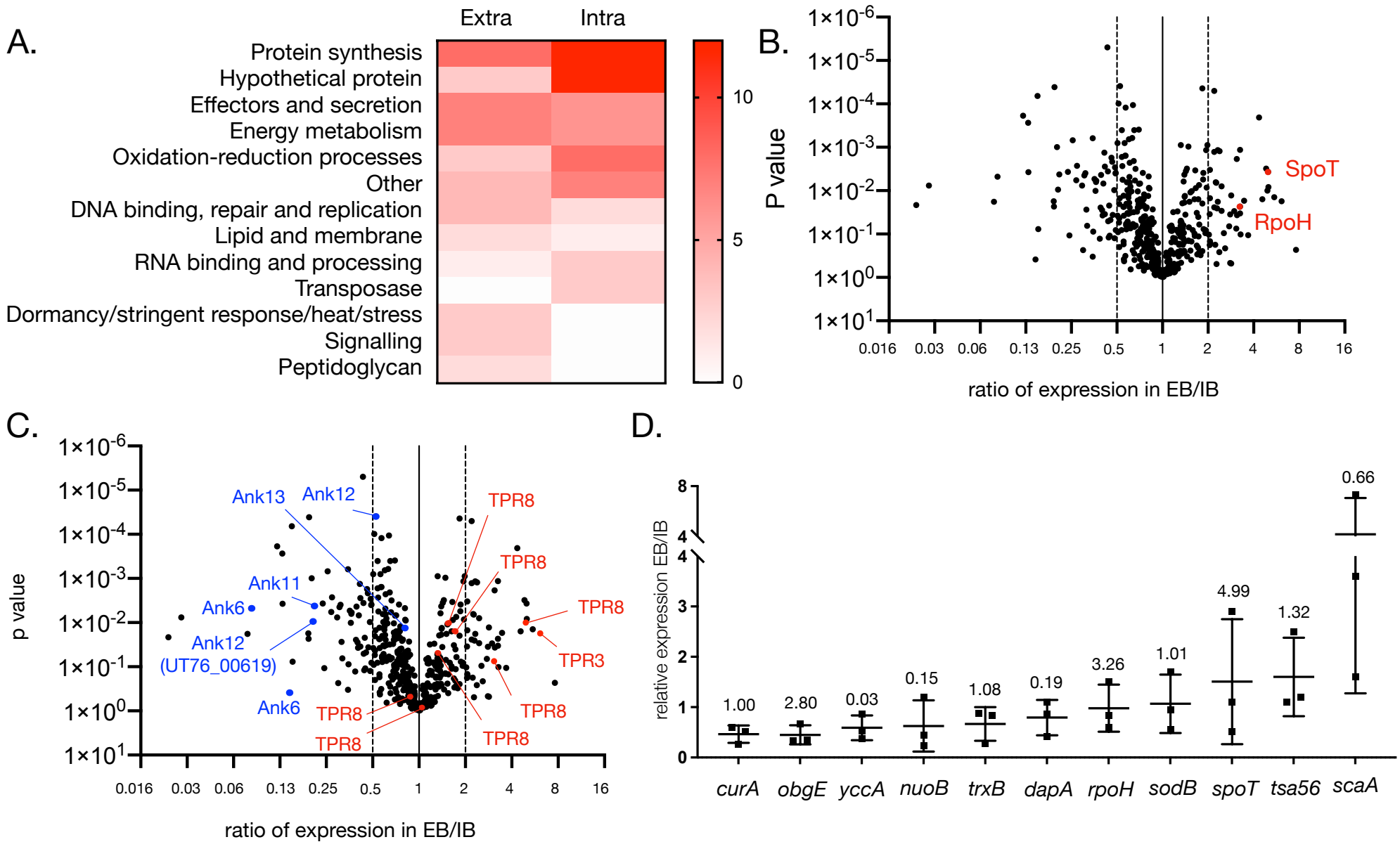

Fig. 2: Intracellular and extracellular forms of Ot have distinct gene expression profiles.
A. Pathway analysis of proteins upregulated >2X between IB and EB forms of Ot (60 proteins in IB, 47 proteins in EB). Bacteria were grown in L929 cells at an MOI of 410:1 and harvested four days post-infection. IB and EB Ot were isolated and analysed by shotgun proteomics. B. SpoT and RpoH are upregulated in EB compared with IB Ot as measured by proteomics described in A. C. Differential expression of Ankyrin-repeat-containing proteins (Anks) and tetratricopeptide repeat-containing proteins (TPR) in EB and IB Ot measured by proteomics, as in A. D. RTqPCR analysis showing relative levels of 12 genes expressed in EB and IB Ot. Bacteria were isolated from L929 cells four days post-infection at an MOI of 672:1, 300:1, and 560:1. The figure depicts results from three independent replicates. Gene expression levels were normalised using three genes: *mipZ*, *ank12*, and *16S.* Mean and standard deviation values are shown. The ratio of protein levels in EB/IB, as found in the proteomics experiment in 2A, is given above each gene for comparison.

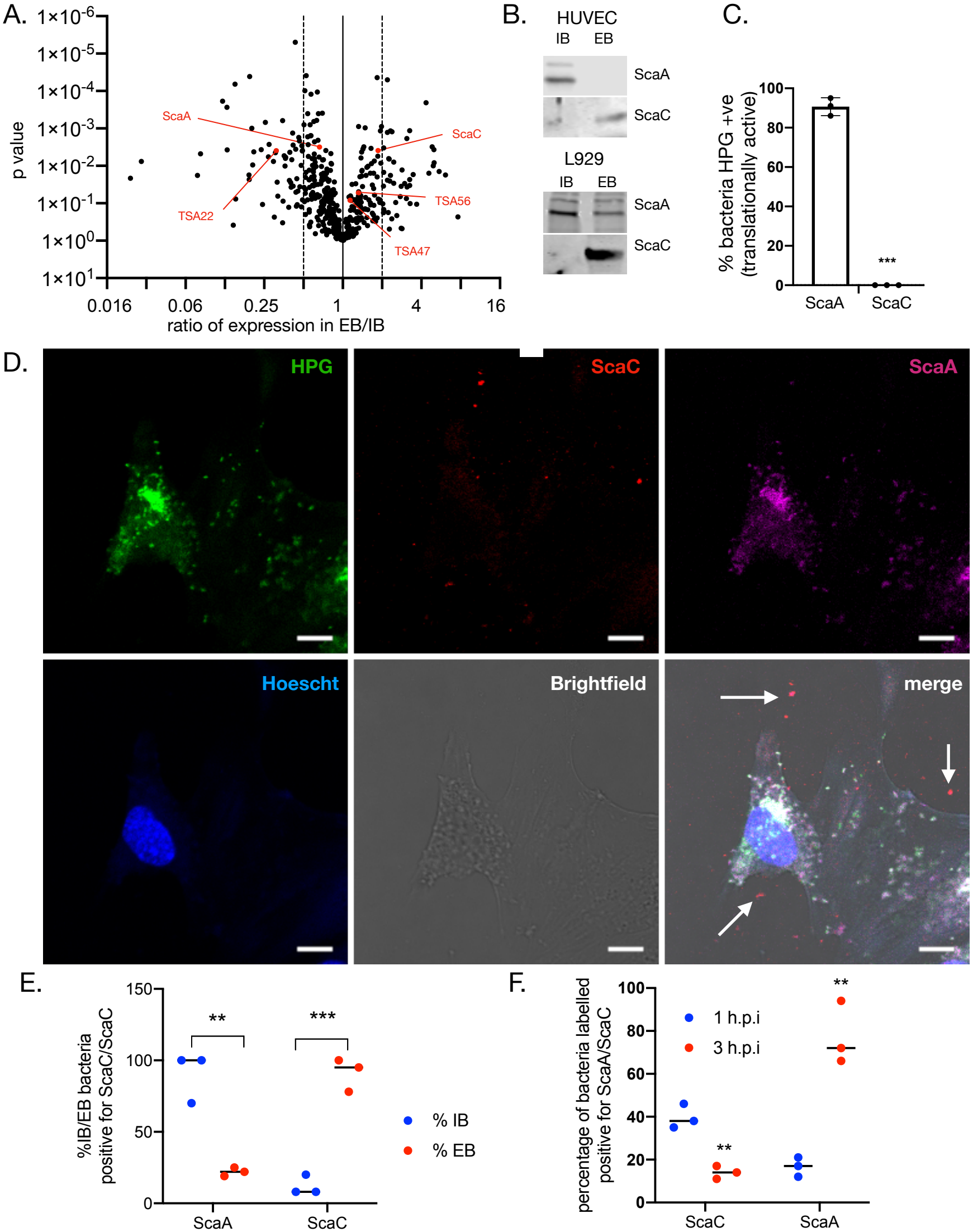

Fig. 3: Autotransporter proteins ScaA and ScaC are differentially expressed on IB and EB forms of Ot.
A. Volcano plot showing differential expression of surface proteins in proteomics analysis of IB and EB forms of Ot. We observed higher expression of ScaC, TSA56, and TSA47 in EB whilst IB Ot expressed higher ScaA and TSA22 levels B. Immunoblot analysis of IB and EB Ot from infected L929 and HUVEC cells confirming differential expression of ScaA, and ScaC between IB and EB forms. Loading was normalised by measuring bacterial genome copy number using qPCR and loading the same number of IB and EB Ot in each pairwise comparison. Uncropped immunoblot images showing antibody specificity are given in Supp. Fig. 3. C. Quantification of translational activity, as determined by a positive confocal microscopy signal observed with the clickable methionine probe L-homopropylgylglycine (HPG). L929 cells were infected with Ot for five days, then fixed and labelled with HPG and anti-ScaA or anti-ScaC antibodies. ScaA/ScaC-positive bacteria were scored as being positive or negative for HPG labelling. Mean and SD of three independent replicates are shown. D. Confocal microscopy images of HUVEC cells infected with Ot for five days and labelled for DNA (hoescht, blue), translational activity (HPG, green), ScaA (anti-ScaA antibody, magenta) and ScaC (anti-ScaC antibody, red). Scale bar = 10 µm. Examples of extracellular bacteria labelled with ScaC are shown with a white arrow. More images as well as equivalent experiments in L929 cells are shown in Supplementary Figures 4 and 5. E. Quantification of confocal micrographs of HUVEC cells infected with Ot and labelled as in 3D. The percentage of IB and EB Ot at five days post-infection that were positively labelled with anti-ScaA and -ScaC antibodies was counted in three independent experiments. Graph shows mean and SD, and p value determine by unpaired t test. F. Quantification of ScaA- and ScaC-positive IB bacteria inside HUVEC cells one and three hours post-infection, showing an increase in ScaA labelling and a decrease in ScaC labelling. * p-value ≤ 0.05, ** p-value ≤ 0.01, *** p-value ≤ 0.001.

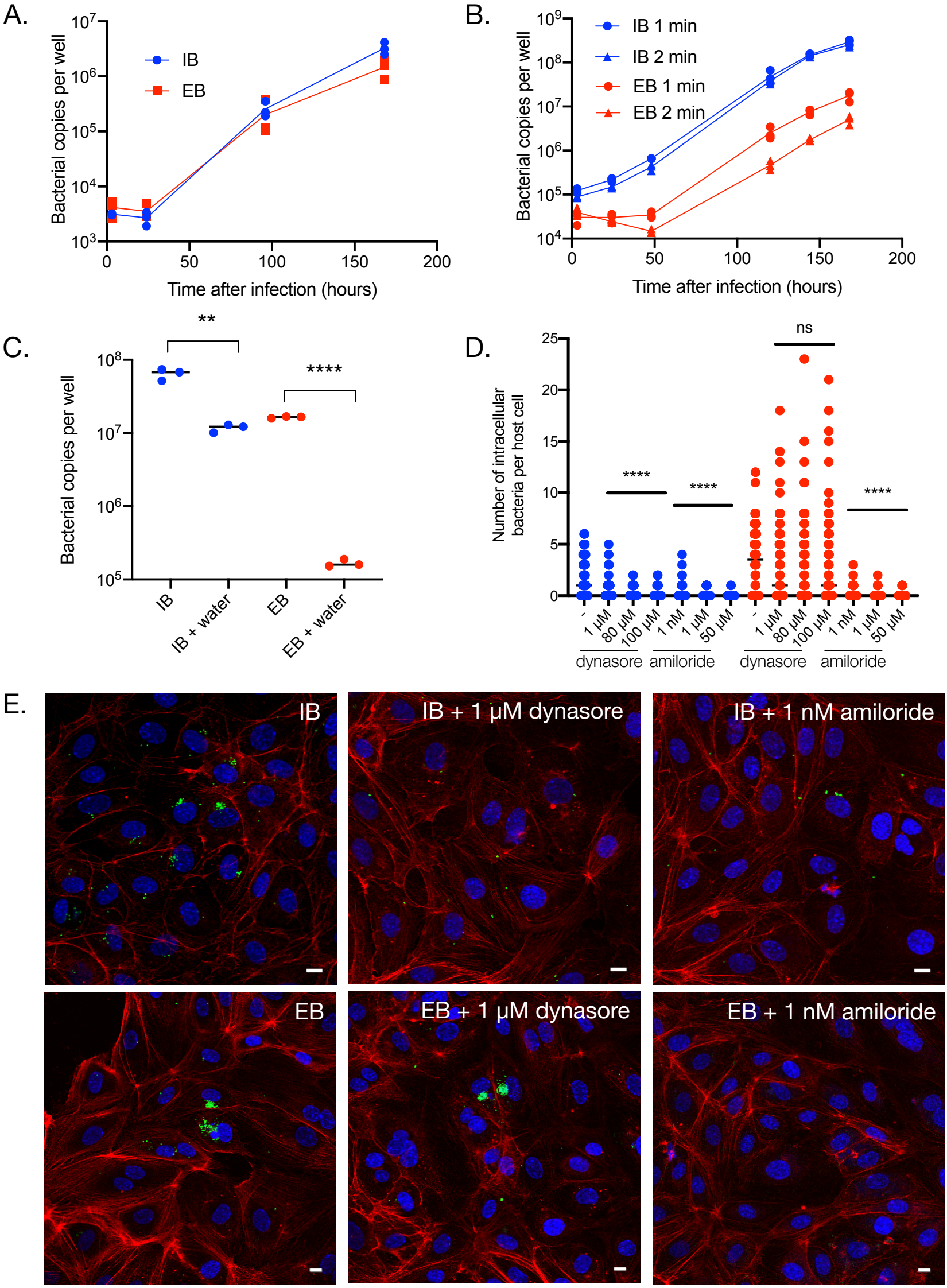

Fig. 4: Both IB and EB populations are infectious but differ in physical stability and mechanism of entry into cells.
A. IB and EB Ot were isolated from infected L929 cells five days post-infection and grown in fresh L929 cells in a 24-well plate. The number of intracellular bacteria was then quantified at 3, 24, 96, and 168 hours post-infection using qPCR against *tsa47,* a single copy Ot gene. Doubling times of IB and EB Ot were similar. B. IB and EB were exposed to physical stress using a bead mill for one or two min; growth was quantified as in 4A. The bead mill did not affect the growth rate of IB Ot but reduced that of EB Ot in an exposure-dependent manner. C. IB and EB were exposed to osmotic shock by suspending the bacteria in water for five min and then growing them in fresh L929 cells. Bacterial copy number after seven days was quantified by qPCR. EB was more susceptible to osmotic shock than IB Ot, as shown by a more significant decrease in bacterial number. D. Quantification of the effect of endocytosis inhibitors on entry of IB and EB Ot. IB and EB were isolated from L929 cells five days post-infection and then seeded onto fresh HUVEC cells that had been treated with inhibitors of clathrin-mediated endocytosis (dynasore) or macropinocytosis (amiloride). Cells were fixed three hours post-infection. Dynasore inhibits entry of IB but not EB, indicating that clathrin-mediated endocytosis is the major mode of entry of this population, whilst amiloride strongly inhibited EB and, to a lesser extent, IB. This observation points to a role for macropinocytosis in EB's entry into mammalian cells. Confocal microscopy images shown in E. Red = actin (phalloidin), blue = hoescht (DNA), green = Ot (anti-TSA56 antibody). Scale bar = 10 μm. Similar results were found in L929 cells (Supp. Fig. 6).

A.

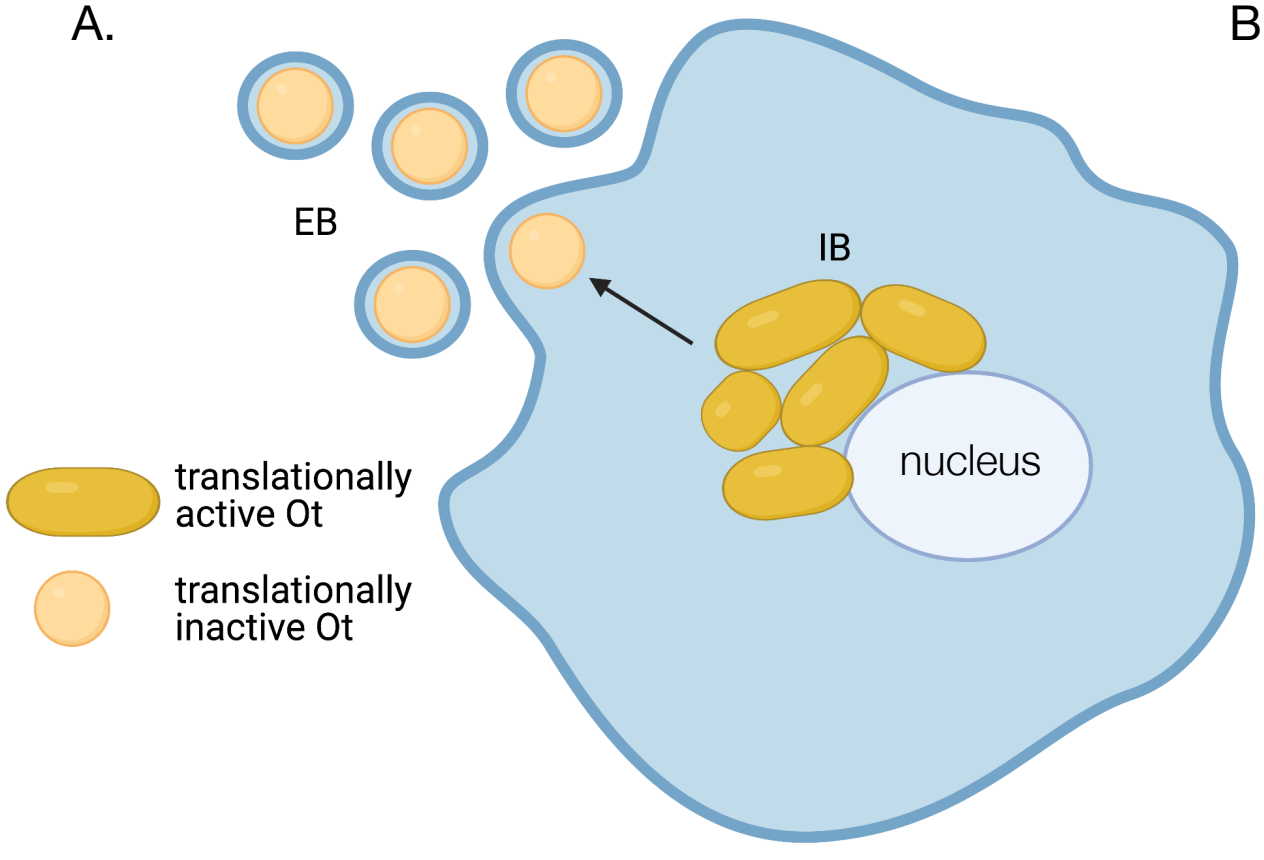

B.

IB	EB
more peptidoglycan	less peptidoglycan
elongated and round	round
less fragile	more fragile
TSA56 less cross linked	TSA56 highly cross linked
translationally active	translationally inactive
high expression of Anks	high expression of TPRs
high ScaA/low ScaC	low ScaA/high ScaC
enters cells by endocytosis	enters cells by macropinocytosis

Fig.5: An overview of the infection cycle of Ot, showing differentiation between IB and EB forms.
IB replicate in a micro-colony adjacent to the nucleus where they are elongated in shape and translationally active. Bacteria move to the cell's edge and transition to an EB form that is round and translationally inactive. Created with BioRender.com B. Table summarizing the differences between IB and EB forms of Ot.